1521-0111/12/8201-97–104$25.00
MOLECULAR PHARMACOLOGY
Copyright © 2012 The American Society for Pharmacology and Experimental Therapeutics
Mol Pharmacol 82:97–104, 2012

Vol. 82, No. 1
78212/3777651

Architecture and Pore Block of Eukaryotic Voltage-Gated Sodium Channels in View of NavAb Bacterial Sodium Channel Structure

Denis B. Tikhonov and Boris S. Zhorov

Sechenov Institute of Evolutionary Physiology and Biochemistry, Russian Academy of Sciences, St. Petersburg, Russia (D.B.T., B.S.Z); and Department of Biochemistry and Biomedical Sciences, McMaster University, Hamilton, Ontario, Canada (B.S.Z.)

Received February 8, 2012; accepted April 9, 2012

ABSTRACT

The X-ray structure of the bacterial sodium channel NavAb provides a new template for the study of sodium and calcium channels. Unlike potassium channels, NavAb contains P2 helices in the outer-pore region. Because the sequence similarity between eukaryotic and prokaryotic sodium channels in this region is poor, the structural similarity is unclear. We analyzed it by using experimental data on tetrodotoxin block of sodium channels. Key tetrodotoxin-binding residues are outer carboxylates in repeats I, II, and IV, three positions downstream from the selectivity-filter residues. In a NavAb-based model of Nav1 channels derived from the sequence alignment without insertions/deletions, the outer carboxylates did not face the pore and therefore did not interact with tetrodotoxin. The hypothesis that the evolutionary appearance of Nav1 channels involved point deletions in an ancestral channel between the selectivity filter and the outer carboxylates allowed building of a NavAb-based model with tetrodotoxin-channel contacts similar to those proposed previously. This hypothesis also allowed us to reproduce in Nav1 the folding-stabilizing contacts between long-side chain residues in P1 and P2, which are seen in NavAb. The NavAb-based inner-pore model of Nav1 preserved major features of our previous KcsA-based models, including the access pathway for ligands through the repeat III/IV interface and their interactions with specific residues. Thus, structural properties of eukaryotic voltage-gated sodium channels that are suggested by functional data were reproduced in the NavAb-based models built by using the unaltered template structure but with adjusted sequence alignment. Sequences of eukaryotic calcium channels aligned with NavAb without insertions/deletions, which suggests that NavAb is a promising basis for the modeling of calcium channels.

Introduction

For more than a decade, structural interpretation of experimental data on calcium and sodium channels was necessarily based on homology models, which were built by using X-ray structures of potassium channels as templates. The recent X-ray structure of the voltage-gated prokaryotic sodium channel NavAb (Payandeh et al., 2011) calls for revisiting atomistic mechanisms proposed for eukaryotic channels, including gating, ion selectivity, ion permeation, and modulation by ligands. This is not a trivial task, because the degree of structural similarity between the homotetrameric prokaryotic channel NavAb and heterotetrameric eukaryotic channels is unclear. An approach to address this fundamental question is to consider a large body of experimental data on mutational analyses, electrophysiological characteristics, and structure-function relationships of ligands in eukaryotic channels in view of the NavAb structure. This should involve homology modeling of eukaryotic Nav1 channels with the NavAb structure as a template.

Comparison of the NavAb structure with that of KcsA (K^+ channel from *Streptomyces lividans)*, which is the best-studied prokaryotic potassium channel crystallized in the closed state and which has been used extensively for homology modeling, shows highly conserved mutual disposition of the pore domain principal components (i.e., S6 inner helices, S5 outer helices, and P1 pore helices) (Fig. 1). Major distinguishing features are selectivity-filter structures, which are generally thought to differ in sodium and potassium channels, and the presence of P2 helices between the selectivity-filter residues and the S6 helices in NavAb. The P2 helices were proposed in a previous model of a bacterial sodium channel,

This work was supported by grants from the Russian Academy of Sciences Molecular and Cell Biology program (to D.B.T.) and the Natural Sciences and Engineering Research Council of Canada [Grant GRPIN/238773-2009] (to B.S.Z.). Computations were made possible by the facilities of the Shared Hierarchical Academic Research Computing Network (http://www.sharcnet.ca).

D.B.T. and B.S.Z. contributed equally to this work.

Article, publication date, and citation information can be found at http://molpharm.aspetjournals.org.
http://dx.doi.org/10.1124/mol.112.078212.

ABBREVIATIONS: MCM, Monte Carlo minimization; 3D, three-dimensional; TTX, tetrodotoxin.

A

```
               ======P1=====        ========= Inner helix =======
                    p41      p51               i11        i21
                    |        |                 |          |
KcsA          YPRAL WWSVETATTV GYGD  RCVAVVV MVAGITSFGL VTAALATWFV
NaVab         LGESF YTLFQVMTLE SWSM  WVFFIPF IFVVTFVMIN LVVAICVDAM
Superposed      *** ********         ******* ********** ******
```

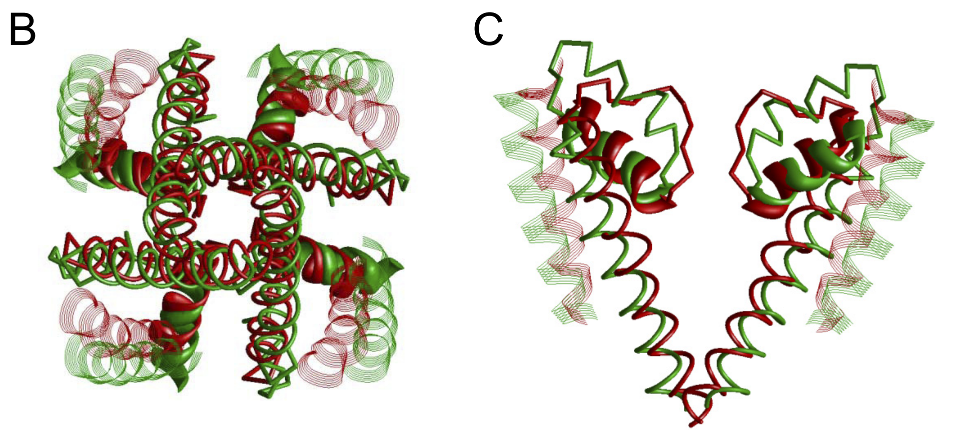

Fig. 1. A, sequence alignment of KcsA and NavAb obtained through superposition of the X-ray structures of these channels. Only fragments of the P-loop sequences and the inner helices are shown. Positions of residues whose root mean square deviations were minimized to obtain the 3D superimposed structures are marked with asterisks. B and C, intracellular and side views, respectively, of the superimposed X-ray structures of KcsA (red) and NavAb (green). The outer helices, P1 helices, and inner helices are shown as strands, ribbons, and rods, respectively. The selectivity filter region in KcsA and the P2 helices in NavAb are shown as α-tracings. The general folding patterns of the channels are clearly similar except for the outer-pore region.

NaChBac (Shafrir et al., 2008), but homology models of eukaryotic sodium and calcium channels that were based on X-ray structures of potassium channels lacked helices immediately downstream from the selectivity filter.

We built a NavAb-based homology model of the eukaryotic sodium channel (the Nav1.4 sequence was used) and docked representative ligands in the outer pore and the central cavity (the inner pore). We used tetrodotoxin (TTX) as the outer-pore blocker and the well studied local anesthetic tetracaine as the inner-pore blocker. We found that all of the data on tetracaine actions that were explained with the KcsA-based model of the closed Nav1.5 channel (Bruhova et al., 2008) were explained in the same way with the NavAb-based model. In contrast, docking of tetrodotoxin in a straightforward NavAb-based model that was based on previously proposed sequence alignments of the P-loop region between potassium and sodium channels failed to explain the available experimental data. The critical discrepancy involved aspartate and glutamate residues three or four positions downstream from the selectivity-filter residues (the outer carboxylates). These carboxylates are generally accepted to interact with TTX, but they were located too far from TTX in the straightforward model, because of their positions in the P2 helices, which do not face the outer pore. To resolve the problem, we proposed that the evolutionary appearance of voltage-gated eukaryotic sodium channels involved point deletions between the selectivity-filter residues and the outer carboxylate in each repeat of an ancestral channel. This hypothesis allowed us to propose a new sequence alignment between NavAb and eukaryotic sodium channels that substantially improved the sequence similarity and to build a new model with stabilizing inter-repeat contacts involving conserved residues in the P1 and P2 helices, which explains available data on TTX binding.

Materials and Methods

All calculations were performed by using ZMM (ZMM Software, Inc., Flamborough, Ontario, Canada). The nonbonded energy was calculated by using the AMBER force field (Weiner et al., 1984, 1986), with a cutoff distance of 8 Å. The hydration energy was calculated by using the implicit solvent method (Lazaridis and Karplus, 1999). Electrostatic interactions were calculated by using the distance-dependent dielectric function. The atomic charges of TTX were calculated by using the semiempirical method AM1 (Dewar et al., 1985) with MOPAC software. The Monte Carlo minimization (MCM) method (Li and Scheraga, 1987) was used to optimize the models. During energy minimizations, the α-carbons of the P-helices were constrained to their corresponding positions in the template by using pins. A pin is a flat-bottomed energy function that allows an atom to deviate up to 1 Å from the template without a penalty and imposes a penalty of 10 kcal $\cdot$ mol^{-1} $\cdot$ Å^{-1} for deviations of >1 Å.

MCM of each model was performed until 2000 consecutive energy minimizations did not decrease the energy of the apparent global minimum. The multi-MCM protocol (Tikhonov and Zhorov, 2007) was used to dock TTX and to impose specific distance constraints. No specific energy terms were used for cation-π interactions, which were accounted for with partial negative charges at the aromatic carbons (Bruhova et al., 2008).

We designated residues by using labels that are universal for P-loop channels (Zhorov and Tikhonov, 2004). A residue label includes the repeat number, which is omitted if all four repeats are meant, the segment index (o, outer helix S5; p, P-loop; i, inner helix S6), and the residue position in the segment (Fig. 1A). Further details of methods can be found elsewhere (Tikhonov and Zhorov, 2007).

Results

Straightforward Outer-Pore Model. Although the sequences of NavAb and KcsA are essentially different, com-

parison of the 3D structures of these channels allows us to propose the unambiguous sequence alignment of P1 and inner helices (Fig. 1). This resolves the longstanding problem of sequence alignment between P1 helices and the selectivity-filter region of potassium and sodium channels and confirms an alignment proposed previously (Zhorov et al., 2001). We used this alignment to minimize the root mean square deviations between α-carbons of residues in positions indicated by stars in Fig. 1. Although the root mean square deviations of α-carbons in the 3D-aligned regions were as large as 2.9 Å, the superposition obtained clearly showed that the general folding patterns for P1 and inner helices are similar.

Unlike KcsA and other potassium channels, NavAb contains P2 helices. The corresponding outer-pore region of eukaryotic channels contains important TTX-sensing residues. Specific interactions of TTX with the outer pore were extensively studied experimentally (see Fozzard and Lipkind, 2010, for review), and these data were used to design TTX-channel models (Lipkind and Fozzard, 1994; Tikhonov and Zhorov, 2005). Here we used TTX as a probe to explore whether the NavAb template could be used to reproduce known experimental data on TTX binding and other properties of the outer pore in eukaryotic channels.

In our homology model (the Nav1.4 sequence was used), which was based on the straightforward alignment (Fig. 2A), the outer pore was wide enough to accommodate TTX. Upon MCM docking, TTX readily established contacts with the selectivity-filter residues Asp-Glu-Lys-Ala (position p50) and neighboring TTX-sensing residues. However, the three outer carboxylates (Glu^{1p53}, Glu^{2p53}, and Asp^{4p53}), whose substitutions strongly affect TTX action (Terlau et al., 1991) and which were proposed in previous models to interact directly with TTX (Lipkind and Fozzard, 1994; Tikhonov and Zhorov, 2005), did not face the pore and were located too far from the ligand (Fig. 2, B and C). Because these residues are located in the P2 helices, their reorientation in the model would require destruction of the helices. In contrast, Asp^{3p54}, which according to experimental data interacts with TTX much more weakly than do the other outer carboxylates (Terlau et al., 1991), faced the pore and approached the ligand (Fig. 2, B and C). Therefore, the model of Nav1 channels that was built with straightforward sequence alignment with NavAb failed to explain experimental data on TTX binding.

An important problem in homology modeling is to detect residues that may be involved in contacts that stabilize protein folding and to ensure that such contacts occur in the model. Previously we proposed that exceptionally conserved tryptophans in position p52 stabilize the 3D structure of the P-loop region by forming inter-repeat hydrogen bonds (Tikhonov and Zhorov, 2011). This proposition is now confirmed by the NavAb structure, in which Trp^{p52} residues indeed form inter-repeat hydrogen bonds. However, hydrogen-bonding partners of these residues are not the same as in our model. In the NavAb X-ray structure, the side chains of tryptophans in position p52 donate inter-repeat hydrogen bonds to side chains of threonines in position p48 but do not expose aromatic rings to the pore, as we suggested.

We also proposed that polar residues in position p45 (P1 helices) should participate in stabilizing the outer-pore structure by forming specific contacts with residues beyond the P1 helices (Tikhonov and Zhorov, 2011). In the NavAb structure, side chains of Gln^{p45} residues are engaged in inter-repeat

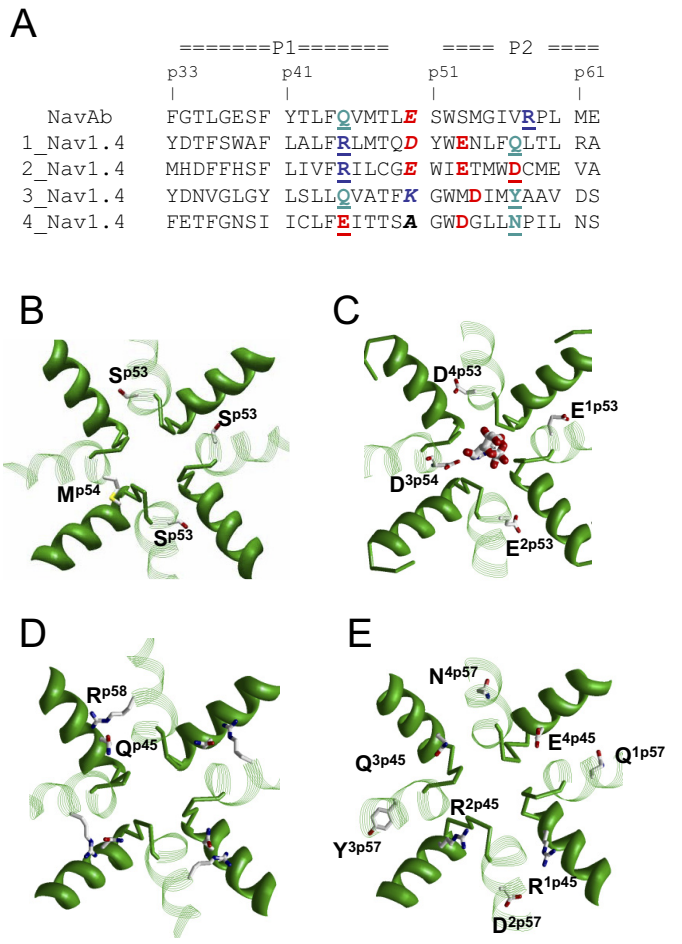

Fig. 2. Straightforward NavAb-based model of the P domain in eukaryotic sodium channels built without deletions between helices P1 and P2. This model cannot reproduce well known data regarding the outer-pore structure, which indicates either that the outer-pore structure is not conserved between NavAb and Nav1 or that the alignment is incorrect. A, straightforward sequence alignment without insertions or deletions. Selectivity-filter residues in position p50, outer-carboxylate residues of Nav1 in positions p53 and p54, and long-chain polar residues in positions p45 and p57-p58 are highlighted. B, extracellular view of the NavAb X-ray structure with side chains in positions Ser^{p53} and Met^{p54}. P1 helices are shown as ribbons, P2 helices as strands, and P1-P2 linkers as rods. Side chains of Ser^{p53} are oriented away from the outer pore, whereas Met^{p54} faces the outer pore. C, straightforward model of Nav1.4 with docked tetrodotoxin. The outer carboxylates Glu^{1p53}, Glu^{2p53}, and Asp^{4p53}, which are known to form contacts with TTX, do not face the pore and therefore cannot form contacts with TTX, whereas Asp^{3p54}, which does not contribute to TTX binding according to experiments, is the only outer carboxylate that faces the pore and interacts with TTX in the model. D, X-ray structure of NavAb with long-chain polar residues Gln^{p45} and Arg^{p58}, which interact with each other. These interactions may contribute to the stability of the P-loop region. E, straightforward model of the Nav1 channel, in which long-chain polar residues in positions p45 and p57 cannot approach each other because the sequences of the repeats are shifted one position toward the N-end, compared with residue p58 in NavAb.

hydrogen bonds with side chains of Arg^{p58} residues in P2 helices (Fig. 2D). Eukaryotic sodium and calcium channels do have highly conserved polar residues in position p45 and seven or eight positions downstream from the selectivity-filter residues. In the straightforward sequence alignment with NavAb, however, polar residues in the P2 helices of Nav1 channels occur in position p57; i.e., they are shifted one position toward the amino end (Fig. 2A). Therefore, in the corresponding homology model, side chains of these polar

residues cannot make specific contacts with polar residues in position p45 (Fig. 2E). Thus, in addition to failing to reproduce the TTX binding data, the straightforward model did not reproduce stabilizing interhelical contacts involving conserved polar residues in the P1 and P2 helices.

Model with Adjusted Sequence Alignment. To resolve the aforementioned problems, we proposed a new sequence alignment between Nav1 and NavAb (Fig. 3A). In this alignment, we introduced gaps in the Nav1.4 sequence at positions where point deletions in an ancestral ion channel probably occurred upon the evolutionary appearance of Nav1 channels. As a result, the loop between the P1 and P2 helices in each repeat of Nav1 is one residue shorter, compared with NavAb. The adjusted sequence alignment has four important consequences. First, exceptionally conserved Trp^{p52} residues, which form inter-repeat hydrogen bonds that stabilize the P-region in the NavAb channel, occurred in the matching positions of all repeats in eukaryotic sodium and calcium channels. Second, highly conserved polar residues in the P2 helices occurred in the matching position p58 in Nav1 and NavAb sequences and thus could participate in stabilizing contacts with residues in position p45 of P1 helices. Third, TTX-sensing outer carboxylates Glu^{1p54}, Glu^{2p54}, and Asp^{4p54} occurred in the matching positions, which face the outer pore in the NavAb structure. (Calcium channels have acidic residues in the same position.) Fourth, an outer carboxylate in repeat III, which does not interact with TTX according to experimental data, occurred in position 3p55, which does not face the pore, and therefore would not interact with TTX in the homology model.

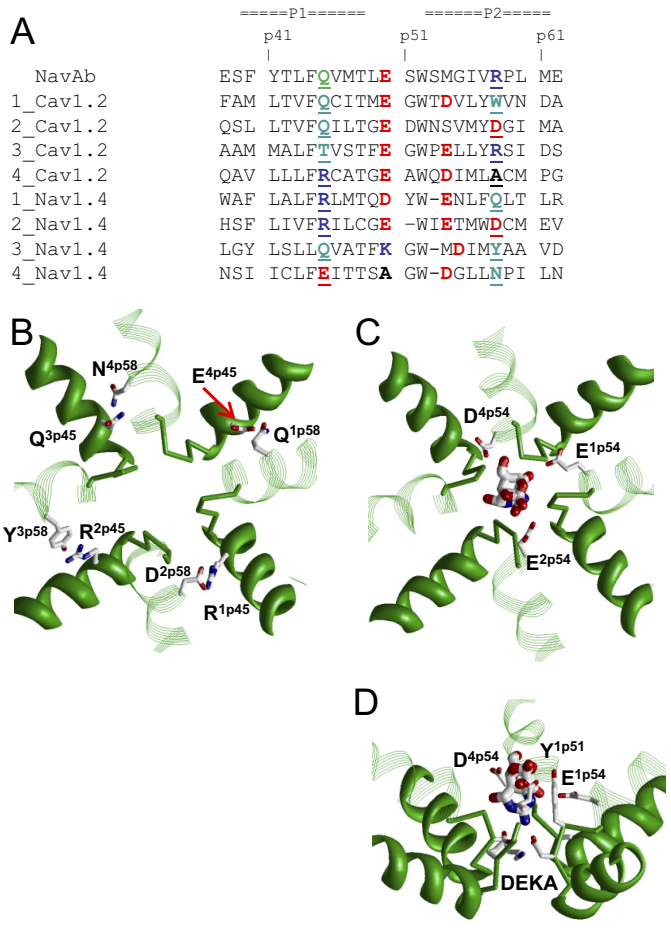

Fig. 3. Adjusted NavAb-based model of the P-loop region of Nav1. A, proposed sequence alignment of NavAb with Cav1.2 and Nav1.4 channels. Critical features of this alignment are the matching positions of pairs of residues p45/p58 and p48/p52, which may be involved in interactions that stabilize the folding of the P-loop region. Unlike Nav1.4, Cav1.2 aligns with NavAb without adjustments, which suggests the evolutionary history. The critical consequence of alignment is the pore-facing orientation of the outer carboxylates, in agreement with experimental data on TTX binding. B, stabilizing contacts between residues in positions p45 and p58. Despite the different chemical natures of the residues, the model suggests specific bonding of each pair. C and D, extracellular (C) and side (D) views of the Nav1.4 model with bound TTX. The model readily reproduces experimental data on TTX-channel interactions, including contacts with the selectivity-filter residues Asp-Glu-Lys-Ala (DEKA) and the outer carboxylates as well as cation-π interactions with Tyr^{1p51}.

We used this alignment to build a new (adjusted), NavAb-based, homology model of Nav1 channels. Because the gaps were proposed in the turn regions of the P1-P2 linkers, it was possible to build the adjusted model without displacing the P2 helices of Nav1 channels relative to the NavAb template. Therefore, α-carbons in the P1 and P2 helices of the adjusted model occupy practically the same positions as matching residues in the NavAb structure. Compared with the straightforward model, all residues in the P2 helices of the adjusted model are reoriented by approximately one fourth of an α-helix turn. An immediate result of the model, which is based on the adjusted sequence alignment, was that intersegment contacts between residues p45 and p58 were readily established with MCM (Fig. 3B). These contacts include a salt bridge (Arg^{1p45}-Asp^{2p58}), a π-stacking contact (Arg^{2p45}-Tyr^{3p58}), and two hydrogen bonds (Gln^{3p45}-Asn^{4p58} and Glu^{4p45}-Gln^{1p58}).

The second critical structural consequence of the proposed gaps in the sequence alignment is that the side chains of three outer carboxylates are exposed in the pore lumen of the adjusted model. The outer carboxylates occurred in 3D positions that are close to the positions of the same residues in our previous models (Tikhonov and Zhorov, 2005, 2011). MCM docking of TTX in the adjusted model yielded a complex with close contacts between TTX and outer carboxylates in repeats I, II, and IV (Fig. 3, C and D). These contacts are a key feature of previous TTX-Nav1.4 models (Lipkind and Fozzard, 1994; Tikhonov and Zhorov, 2005, 2011). Furthermore, π-cation interactions between TTX and Tyr^{1p51} (Santarelli et al., 2007) were readily reproduced in the adjusted model. Thus, the proposed gaps in the Nav1 sequence aligned with NavAb and calcium channels (Fig. 3A) improved the sequence similarity and allowed us to build the adjusted homology model, which explains the available TTX binding data as well as the presence of highly conserved residues that form specific inter-repeat contacts with each other to stabilize the folding of the P-loop region.

Inner-Pore Model. The sequence alignment of the inner helices of KcsA with the S6 segments of NavAb is obviously dictated by the superimposition of the X-ray structures. The sequence similarity of NavAb to eukaryotic sodium channels is clear from the alignment shown in Fig. 4A. Our homology modeling of the inner-pore region did not face the problems we encountered when we modeled the outer pore. Local anesthetics are well studied inner-pore blockers of sodium channels (e.g., Chahine et al., 1992; Yarov-Yarovoy et al., 2001, 2002; Kondratiev and Tomaselli, 2003; Nau and Wang,

MOL PHARM
MOLECULAR PHARMACOLOGY

A

```
               ======P1======          ======== Inner helix S6 =====
                    p40       p50              i11          i21
                     |         |                |            |
   KcsA     LITYPRAL WWSVETATTV    RCVAVVV MVAGITSFGL VTAALATWFV
   NavAb    FGTLGESF YTLFQVMTLE    WVFFIPF IFVVTFVMIN LVVAICVDAM
1_Nav1.4    YDTFSWAF LALFRLMTQD    MIFFVVI IFLGSFYLIN LILAVVAMAY
2_Nav1.4    MHDFFHSF LIVFRILCGE    LTVFLMV MVIGNLVVLN LFLALLLSSF
3_Nav1.4    YDNVGLGY LSLLQVATFK    YLYFVIF IIFGSFFTLN LFIGVIIDNF
4_Nav1.4    FETFGNSI ICLFEITTSA    ICFFCSY IIISFLIVVN MYIAIILENF
```

B C D E

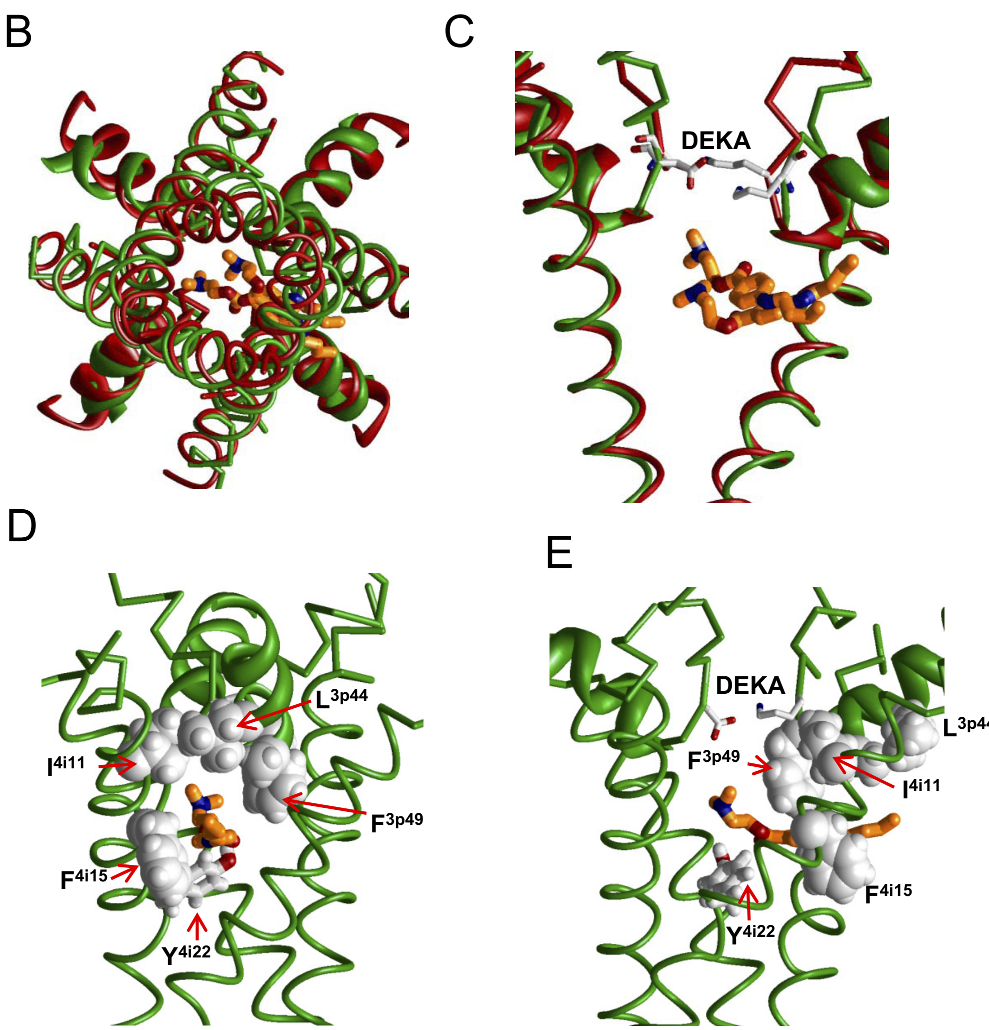

Fig. 4. Local anesthetic tetracaine in the inner pore of the closed Nav1 channel. A, aligned sequences of KcsA, NavAb, and Nav1.4 channels. Bold type indicates selectivity filter residues. Residues that control the access and binding of local anesthetics in the closed Nav1 channels are underlined. Tetracaine-sensing residues Phe^{4i15} and Tyr^{4i22} are green. B, cytoplasmic view of the superimposed KcsA-based (red) and NavAb-based (green) models of Nav1. For clarity, S5 helices not shown. Tetracaine is shown as rods with red oxygens, blue nitrogens, and orange carbons. C, side view of the superposition in B with two repeats removed for clarity and the selectivity-filter residues shown as sticks. Despite some differences in the details of the models, the positions of the selectivity-filter residues are very similar. The hands-free protocol for MCM docking predicted essentially the same position and orientation of tetracaine in the two models. The major features of this binding mode include the location of the ligand ammonium group at the focus of P1 helices and exposure of the hydrophobic tail in the hydrophobic access pathway between repeats III and IV. DEKA, selectivity-filter residues Asp-Glu-Lys-Ala. D and E, orthogonal side views of the NavAb-based model of Nav1.4. A local anesthetic-sensing residue Tyr^{4i22} is shown as sticks. Some residues that control the hydrophobic access pathway to the closed channels are space-filled (Bruhova et al., 2008). The latter group includes a well known local anesthetic-sensing residue Phe^{4i15}.

2004; Fozzard et al., 2011). The key local anesthetic-sensing residues are Phe^{4i15} and Tyr^{4i22} in the S6 segment of repeat IV and Phe^{3p49} in the P-loop turn. Deviations of the α-carbons of these residues between the NavAb-based model and the KcsA-based model (Bruhova et al., 2008) were 3.1, 2.1, and 2.2 Å, respectively.

We docked tetracaine in the inner pore as described previously (Bruhova et al., 2008). The docking yielded a low-energy ligand-channel complex (Fig. 4, B and C) with the horizontal orientation of tetracaine. The same binding mode was predicted in the KcsA-based model of Nav1.5 with tetracaine (Bruhova et al., 2008). The ammonium group of the ligand occurred near the focus of P1 helices, whereas the aromatic group extended in the repeat III/IV interface. The ligand slightly interacts with Tyr^{4i22}, which is located at the inner-pore narrowing. Only the terminal hydroxyl of Tyr^{4i22} reached the tetracaine molecule. The uncharged part of tetracaine experiences van der Waals interactions with Phe^{4i15}. All of these results are in agreement with the experimentally revealed roles of Tyr^{4i22} and Phe^{4i15} (Li et al., 1999; Ahern et al., 2008). Despite the aforementioned root mean square deviation between the X-ray structures of KcsA and NavAb, similar tetracaine-binding models were obtained for KcsA- and NavAb-based homology models of Nav1 channels. Therefore, the differences in the inner-pore regions of different homology models should be considered noncritical, as long as the principal features of the channel-tetracaine complex are concerned.

In addition to the S6 segments, residues in the selectivity filter and P-turns, which link the P1 helices to the selectivity-filter residues, are important for the binding of different ligands in the inner pore (Wang et al., 2006; Tikhonov and Zhorov, 2007). The 3D disposition of the P1 helices, P-turns, and selectivity-filter Asp-Glu-Lys-Ala residues in the NavAb-based model of Nav1 channels is similar to that proposed in our earlier model of the sodium channel (Tikhonov and Zhorov, 2005; Bruhova et al., 2008). The differences in the outer-pore structure (between the present and previous models) do not significantly affect the local anesthetic binding mode and pattern of ligand-channel interactions obtained. We also performed tetracaine docking with the model in which the outer pore was modeled without proposed deletions. No significant difference was found (data not shown). This is not surprising, because the ammonium group of tetracaine is as far as ~15 Å from the acidic residues in the outer pore.

Access Pathway for Ligands into Inner Pore of Closed Nav1 Channel. Lipophilic ligands can reach the binding site in the inner pore of closed channels through the "hydrophobic pathway" (Hille, 1977). In some channels, this pathway is accessible also for charged ligands (Qu et al., 1995; Lee et al., 2001). Earlier, we proposed that ligands may access closed sodium and calcium P-loop channels through a pathway between S6 helices in repeats III and IV and along the P1 helix in repeat III (Yamaguchi et al., 2003; Tikhonov and Zhorov, 2005; Tikhonov et al., 2006; Bruhova et al., 2008). Such a pathway can now be clearly seen in the NavAb structure, where the gap between the three helices is even wider than in KcsA, which was used as a template for our previous homology models. Residues whose mutations affect ligands' ingress into and egress from the closed sodium and calcium channels do line the repeat IIIP1-IIIS6-IVS6 interface in both KcsA-based (Bruhova et al., 2008) and NavAb-based (Fig. 4, D and E) models of Nav1 channels. Thus, our structural interpretations of experimental data regarding the access and binding of inner-pore ligands in the closed sodium channels do not need revisions in view of the NavAb structure.

Discussion

Despite the significant progress in structural biology of ion channels, the number of available X-ray structures is still rather small and many important observations from functional studies lack structural interpretations. The necessity of such interpretations is obvious for asymmetric eukaryotic channels, including calcium and sodium channels, which are targets for many drugs and toxins. Computer-based homology modeling remains a major approach to predicting structural features of noncrystallized ion channels, including ligand binding to these channels. New X-ray structures increase the number of structural problems that can be addressed with homology modeling and motivate reexamination of propositions based on previous homology models. The major goal of the present study was to explore whether the X-ray structure of the prokaryotic sodium channel NavAb could be used to explain experimental data on eukaryotic sodium channels, particularly data on the actions of TTX and local anesthetics on the sodium channels.

We conclude that the available data on the binding of tetracaine (and probably other local anesthetics) in closed sodium channels and the hydrophobic access pathway into closed channels are in complete agreement with the NavAb structure. The NavAb-based model of the inner pore is very similar to that elaborated by us on the basis of the structure of the closed potassium channel KcsA (Bruhova et al., 2008). However, attempts to dock TTX in the straightforward NavAb-based model of the eukaryotic sodium channel, which is based on published alignments, were unsuccessful. In particular, well known data on the interactions of TTX with outer carboxylates (see Fozzard and Lipkind, 2010, for review), were inconsistent with the straightforward model. In addition, the straightforward model did not reproduce specific inter-repeat contacts between long-chain residues in the P1 and P2 helices that are seen in the X-ray structure of NavAb. A possible conclusion from the straightforward model would be that the outer-pore structures are not conserved between prokaryotic and eukaryotic sodium channels. However, our proposition that the evolutionary appearance of the eukaryotic sodium channels involved deletions in an ancestral channel between the selectivity-filter residues and the P2 helices allowed us to build the adjusted model, which resolved the problems.

Comparison of the X-ray structures of the closed potassium channels KcsA (Doyle et al., 1998), KirBac1.1 (Kuo et al., 2003), and MlotiK1 (Clayton et al., 2008), sodium channel NavAb (Payandeh et al., 2011), and cation-selective glutamate-gated channel GluA2 (Sobolevsky et al., 2009) demonstrates a much higher degree of 3D similarity than expected, given dramatically different sequences and properties of these channels. The common features in the pore-domain folding of these channels are probably ensured through specific stabilizing contacts.

The NavAb, Cav1, and Nav1 channels have highly conserved, putative structure-stabilizing residues in similar but not matching positions of the sequences aligned without insertions/deletions (Fig. 3A). We suggested that the pore domains of these channels have conserved 3D disposition of elements that stabilize the folding of the P-loop region. Therefore, to resolve the inconsistency of the straightforward model of NavAb with experimental data, we did not attempt to rearrange the structural elements (e.g., through shifting, turning, or bulging in the P2 helices). Instead, we proposed a deletion in the flexible linker between the P1 and P2 helices, which did not change the 3D disposition of the major structural elements of the P-loop domain (Fig. 3A).

It is generally recognized that sequence alignment is a crucial step in homology modeling. The adjusted sequence alignment (Fig. 4A) is not the obvious one if only sequence similarities are taken into consideration. It is our understanding that residues in positions p45 and p58 should interact with each other to stabilize NavAb folding, which prompted us to keep these residues in the matching positions of the aligned sequences. This example shows that structural data may have dominant roles in the elaboration of correct sequence alignments (which are of obvious importance for understanding molecular evolution) and, conversely, correct alignments are crucial for modeling of the 3D structures of proteins.

Our study suggests that eukaryotic sodium channels also have P2 helices but the loop between the P1 and P2 helices is one residue shorter, compared with NavAb. These results should help investigators to address structural aspects of the

action of μ-conotoxins, another class of sodium cannel inhibitors. The experimental background for future modeling studies includes data on specific interactions of μ-conotoxins with sodium channels (McArthur et al., 2009) and intriguing effects such as incomplete block by some toxin mutants (Becker et al., 1992) and synergetic action of μ-conotoxin KIIIA and TTX (Zhang et al., 2009). However, understanding of the atomistic mechanisms of conotoxin action is still incomplete. Previous attempts to dock μ-conotoxins with experimentally derived constraints (Choudhary et al., 2007; McArthur et al., 2011a,b) were performed by using homology models in which the outer-pore folding and the location of the selectivity filter in the outer pore appeared inconsistent with the NavAb structure. The important problem of modeling complexes of sodium channels with conotoxins can be now revisited by using the available experimental constraints, the NavAb template, and the proposed sequence alignment of NavAb with eukaryotic sodium channels.

It is now widely accepted that slow-inactivation gating in potassium and sodium channels involves structural rearrangement in the outer pore. Elucidation of the nature of such rearrangements and the contributions of individual residues in stabilizing ion-permeant and impermeant (inactivated) states requires knowledge of the outer-pore structure. The X-ray structures of potassium channels and NavAb show strong contacts between the S1-S4 gating domain and the S5-P-S6 pore domain in the extracellular face of P-loop channels. Experiments revealed coupling between the voltage sensor movement and the outer-pore conformations. In particular, a contact between S1 and pore helices affects the gating properties of potassium channels (Lee et al., 2009). A recent study demonstrated that the domain IV voltage sensor and the outer pore of the sodium channel are conformationally coupled; trapping of the outer pore in a specific conformation with TTX or a disulfide cross-bridge impedes the voltage sensor returning to its resting conformation (Capes et al., 2012). Structural interpretations of these data require full-fledged models of eukaryotic sodium channels. Our model of the outer pore is a step toward this goal.

The consistency of the NavAb-based homology model of Nav1 channels with various experimental data suggests that the secondary structural elements, including P2 helices and stabilizing contacts between the P1 and P2 helices, are conserved between NavAb and eukaryotic sodium channels. The P1-P2 linker in NavAb is probably a good template for modeling eukaryotic calcium channels. Calcium channels, which contain a glutamate residue in position p50 of each repeat, align with the NaChBac channel without insertions/deletions in the P1-P2 region, as was proposed (Durell and Guy, 2001; Ren et al., 2001), and triple substitutions in the NaChBac channel ($E^{p50}D/S^{p51}D/S^{p54}D$) render its calcium selectivity (Yue et al., 2002). Important issues to be addressed in future studies include the mechanism of calcium selectivity and permeation as well as possible roles of outer carboxylates, absolutely conserved aspartate Asp^{2p51}, and positively charged amino ends of the P2 helices.

Authorship Contributions

Participated in research design: Tikhonov and Zhorov.
Conducted experiments: Tikhonov.
Performed data analysis: Tikhonov and Zhorov.
Wrote or contributed to the writing of the manuscript: Tikhonov and Zhorov.

References

Ahern CA, Eastwood AL, Dougherty DA, and Horn R (2008) Electrostatic contributions of aromatic residues in the local anesthetic receptor of voltage-gated sodium channels. *Circ Res* **102:**86–94.
Becker S, Prusak-Sochaczewski E, Zamponi G, Beck-Sickinger AG, Gordon RD, and French RJ (1992) Action of derivatives of mu-conotoxin GIIIA on sodium channels. Single amino acid substitutions in the toxin separately affect association and dissociation rates. *Biochemistry* **31:**8229–8238.
Bruhova I, Tikhonov DB, and Zhorov BS (2008) Access and binding of local anesthetics in the closed sodium channel. *Mol Pharmacol* **74:**1033–1045.
Capes DL, Arcisio-Miranda M, Jarecki BW, French RJ, and Chanda B (2012) Gating transitions in the selectivity filter region of a sodium channel are coupled to the domain IV voltage sensor. *Proc Natl Acad Sci USA* **109:**2648–2653.
Chahine M, Chen LQ, Barchi RL, Kallen RG, and Horn R (1992) Lidocaine block of human heart sodium channels expressed in *Xenopus* oocytes. *J Mol Cell Cardiol* **24:**1231–1236.
Choudhary G, Aliste MP, Tieleman DP, French RJ, and Dudley SC Jr (2007) Docking of mu-conotoxin GIIIA in the sodium channel outer vestibule. *Channels (Austin)* **1:**344–352.
Clayton GM, Altieri S, Heginbotham L, Unger VM, and Morais-Cabral JH (2008) Structure of the transmembrane regions of a bacterial cyclic nucleotide-regulated channel. *Proc Natl Acad Sci USA* **105:**1511–1515.
Dewar MJS, Zoebisch EG, Healy EF, and Stewart JJP (1985) Development and use of quantum mechanical molecular models. 76. AM1: a new general purpose quantum mechanical molecular model. *J Am Chem Soc* **107:**3902–3909.
Doyle DA, Morais Cabral J, Pfuetzner RA, Kuo A, Gulbis JM, Cohen SL, Chait BT, and MacKinnon R (1998) The structure of the potassium channel: molecular basis of K^+ conduction and selectivity. *Science* **280:**69–77.
Durell SR and Guy HR (2001) A putative prokaryote voltage-gated Ca^{2+} channel with only one 6TM motif per subunit. *Biochem Biophys Res Commun* **281:**741–746.
Fozzard HA and Lipkind GM (2010) The tetrodotoxin binding site is within the outer vestibule of the sodium channel. *Mar Drugs* **8:**219–234.
Fozzard HA, Sheets MF, and Hanck DA (2011) The sodium channel as a target for local anesthetic drugs. *Front Pharmacol* **2:**68.
Hille B (1977) Local anesthetics: hydrophilic and hydrophobic pathways for the drug-receptor reaction. *J Gen Physiol* **69:**497–515.
Kondratiev A and Tomaselli GF (2003) Altered gating and local anesthetic block mediated by residues in the I-S6 and II-S6 transmembrane segments of voltage-dependent Na^+ channels. *Mol Pharmacol* **64:**741–752.
Kuo A, Gulbis JM, Antcliff JF, Rahman T, Lowe ED, Zimmer J, Cuthbertson J, Ashcroft FM, Ezaki T, and Doyle DA (2003) Crystal structure of the potassium channel KirBac1.1 in the closed state. *Science* **300:**1922–1926.
Lazaridis T and Karplus M (1999) Effective energy function for proteins in solution. *Proteins* **35:**133–152.
Lee PJ, Sunami A, and Fozzard HA (2001) Cardiac-specific external paths for lidocaine, defined by isoform-specific residues, accelerate recovery from use-dependent block. *Circ Res* **89:**1014–1021.
Lee SY, Banerjee A, and MacKinnon R (2009) Two separate interfaces between the voltage sensor and pore are required for the function of voltage-dependent K^+ channels. *PLoS Biol* **7:**e47.
Li HL, Galue A, Meadows L, and Ragsdale DS (1999) A molecular basis for the different local anesthetic affinities of resting versus open and inactivated states of the sodium channel. *Mol Pharmacol* **55:**134–141.
Li Z and Scheraga HA (1987) Monte Carlo-minimization approach to the multiple-minima problem in protein folding. *Proc Natl Acad Sci USA* **84:**6611–6615.
Lipkind GM and Fozzard HA (1994) A structural model of the tetrodotoxin and saxitoxin binding site of the Na^+ channel. *Biophys J* **66:**1–13.
McArthur JR, Singh G, McMaster D, Winkfein R, Tieleman DP, and French RJ (2011a) Interactions of key charged residues contributing to selective block of neuronal sodium channels by μ-conotoxin KIIIA. *Mol Pharmacol* **80:**573–584.
McArthur JR, Singh G, O'Mara ML, McMaster D, Ostroumov V, Tieleman DP, and French RJ (2011b) Orientation of μ-conotoxin PIIIA in a sodium channel vestibule, based on voltage dependence of its binding. *Mol Pharmacol* **80:**219–227.
McArthur JR, Zhang MM, Azam L, Luo S, Olivera BM, Yoshikami D, Bulaj G, Levinson SR, and French RJ (2009) Molecular determinants of μ-conotoxin KIIIA block of voltage-gated sodium channels. *Biophys J* **96:**248a.
Nau C and Wang GK (2004) Interactions of local anesthetics with voltage-gated Na^+ channels. *J Membr Biol* **201:**1–8.
Payandeh J, Scheuer T, Zheng N, and Catterall WA (2011) The crystal structure of a voltage-gated sodium channel. *Nature* **475:**353–358.
Qu Y, Rogers J, Tanada T, Scheuer T, and Catterall WA (1995) Molecular determinants of drug access to the receptor site for antiarrhythmic drugs in the cardiac Na^+ channel. *Proc Natl Acad Sci USA* **92:**11839–11843.
Ren D, Navarro B, Xu H, Yue L, Shi Q, and Clapham DE (2001) A prokaryotic voltage-gated sodium channel. *Science* **294:**2372–2375.
Santarelli VP, Eastwood AL, Dougherty DA, Horn R, and Ahern CA (2007) A cation-pi interaction discriminates among sodium channels that are either sensitive or resistant to tetrodotoxin block. *J Biol Chem* **282:**8044–8051.
Shafrir Y, Durell SR, and Guy HR (2008) Models of the structure and gating mechanisms of the pore domain of the NaChBac ion channel. *Biophys J* **95:**3650–3662.
Sobolevsky AI, Rosconi MP, and Gouaux E (2009) X-ray structure, symmetry and mechanism of an AMPA-subtype glutamate receptor. *Nature* **462:**745–756.
Terlau H, Heinemann SH, Stühmer W, Pusch M, Conti F, Imoto K, and Numa S (1991) Mapping the site of block by tetrodotoxin and saxitoxin of sodium channel II. *FEBS Lett* **293:**93–96.

Tikhonov DB, Bruhova I, and Zhorov BS (2006) Atomic determinants of state-dependent block of sodium channels by charged local anesthetics and benzocaine. *FEBS Lett* **580:**6027–6032.
Tikhonov DB and Zhorov BS (2005) Modeling P-loops domain of sodium channel: homology with potassium channels and interaction with ligands. *Biophys J* **88:** 184–197.
Tikhonov DB and Zhorov BS (2007) Sodium channels: ionic model of slow inactivation and state-dependent drug binding. *Biophys J* **93:**1557–1570.
Tikhonov DB and Zhorov BS (2011) Possible roles of exceptionally conserved residues around the selectivity filters of sodium and calcium channels. *J Biol Chem* **286:**2998–3006.
Wang SY, Mitchell J, Tikhonov DB, Zhorov BS, and Wang GK (2006) How batrachotoxin modifies the sodium channel permeation pathway: computer modeling and site-directed mutagenesis. *Mol Pharmacol* **69:**788–795.
Weiner SJ, Kollman PA, Case DA, Singh UC, Ghio C, Alagona G, Profeta S, and Weiner P (1984) A new force field for molecular mechanical simulation of nucleic acids and proteins. *J Am Chem Soc* **106:**765–784.
Weiner SJ, Kollman PA, Nguyen DT, and Case DA (1986) An all atom force field for simulations of proteins and nucleic acids. *J Comput Chem* **7:**230–252.
Yamaguchi S, Zhorov BS, Yoshioka K, Nagao T, Ichijo H, and Adachi-Akahane S (2003) Key roles of Phe1112 and Ser1115 in the pore-forming IIIS5–S6 linker of L-type Ca^{2+} channel α1C subunit (CaV 1.2) in binding of dihydropyridines and action of Ca^{2+} channel agonists. *Mol Pharmacol* **64:**235–248.
Yarov-Yarovoy V, Brown J, Sharp EM, Clare JJ, Scheuer T, and Catterall WA (2001) Molecular determinants of voltage-dependent gating and binding of pore-blocking drugs in transmembrane segment IIIS6 of the Na^+ channel α subunit. *J Biol Chem* **276:**20–27.
Yarov-Yarovoy V, McPhee JC, Idsvoog D, Pate C, Scheuer T, and Catterall WA (2002) Role of amino acid residues in transmembrane segments IS6 and IIS6 of the Na^+ channel α subunit in voltage-dependent gating and drug block. *J Biol Chem* **277:**35393–35401.
Yue L, Navarro B, Ren D, Ramos A, and Clapham DE (2002) The cation selectivity filter of the bacterial sodium channel, NaChBac. *J Gen Physiol* **120:**845–853.
Zhang MM, McArthur JR, Azam L, Bulaj G, Olivera BM, French RJ, and Yoshikami D (2009) Synergistic and antagonistic interactions between tetrodotoxin and muconotoxin in blocking voltage-gated sodium channels. *Channels* (*Austin*) **3:**32–38.
Zhorov BS, Folkman EV, and Ananthanarayanan VS (2001) Homology model of dihydropyridine receptor: implications for L-type Ca^{2+} channel modulation by agonists and antagonists. *Arch Biochem Biophys* **393:**22–41.
Zhorov BS and Tikhonov DB (2004) Potassium, sodium, calcium and glutamate-gated channels: pore architecture and ligand action. *J Neurochem* **88:**782–799.

Address correspondence to: Boris S. Zhorov, Department of Biochemistry and Biomedical Sciences, McMaster University, 1280 Main Street West, Hamilton, Ontario, L8S 4K1 Canada. E-mail: zhorov@mcmaster.ca